$\varepsilon^{(j)}$ and ξ_l can be solved by (II-10) and (II-11) and then $R_{g'}$ can be solved by (II-12). Although the process as shown here is harder than that for the planar-surface matching, the 2D periodic non-planar-surface matching in principle can be done. In other words, the Bloch-wave method can also be applied to all kinds of periodic planar- or non-planar-surface models.

References

COLELLA, R. (1972). *Acta Cryst.* **A28**, 11-15.
COWLEY, J. M. & MOODIE, A. F. (1957). *Acta Cryst.* **10**, 609-619.
COWLEY, J. M. & MOODIE, A. F. (1959). *Acta Cryst.* **12**, 353-359.
ISHIZUKA, K. & UYEDA, N. (1977). *Acta Cryst.* **A33**, 740-749.
KAMBE, K. (1988). *Acta Cryst.* **A44**, 885-890.
MA, Y. (1990*a*). *Proc. XII Int. Congr. for Electron Microscopy, Seattle*, Vol. 2, pp. 372-373. San Francisco Press.
MA, Y. (1990*b*). *Proc. XII Int. Congr. for Electron Microscopy, Seattle*, Vol. 2, pp. 374-375. San Francisco Press.
MA, Y. & MARKS, L. D. (1989). *Acta Cryst.* **A45**, 174-182.
MA, Y. & MARKS, L. D. (1990*a*). *Acta Cryst.* **A46**, 11-32.
MA, Y. & MARKS, L. D. (1990*b*). *Acta Cryst.* **A46**, 594-606.
MA, Y. & MARKS, L. D. (1991). Submitted to *J. Electron. Microsc. Tech.*
MAKSYM, P. A. & BEEBY, J. L. (1981). *Surf. Sci.* **110**, 423-436.
MARKS, L. D. & MA, Y. (1988). *Acta Cryst.* **A44**, 392-393.
METHERELL, A. J. (1975). *Electron Microscopy in Materials Science*, edited by U. VALDRE & E. RUEDL, Vol. 2, pp. 401-550. Luxembourg: Commission of the European Communities.
MOON, A. R. (1972). *Z. Naturforsch. Teil A*, **27**, 390-401.
PENG, L. M. & COWLEY, J. M. (1986). *Acta Cryst.* **A42**, 545-552.
SHINOHARA, K. (1932). *Inst. Phys. Chem. Res. (Tokyo)*, **18**, 223-236.

Acta Cryst. (1991). A47, 715-723

Structure Retrieval in HREM

BY M. A. GRIBELYUK*

Institute of Crystallography, USSR Academy of Sciences, Leninskii Prospekt 59, 117333 *Moscow, USSR*

(*Received* 25 *June* 1990; *accepted* 17 *May* 1991)

Abstract

A new iteration method for direct structure retrieval starting from the exit plane-wave function $\Psi_e(\mathbf{r})$ is proposed and tested on models. The imaginary part of the potential cannot be retrieved. The effects of the limited resolution of $\Psi_e(\mathbf{r})$ as well as neglect of high-order Laue-zone effects and the choice of the starting potential on the result are discussed. The procedure is found to be preferable to that based on the subsequent approximation method with respect to a higher convergence rate. It is shown that an error as low as 10% may be obtained for the real part of the retrieved potential up to $|\sigma V(\mathbf{r})t| < 5$.

1. Introduction

As is well known, the image-formation process in high-resolution electron microscopy (HREM) is influenced by dynamical scattering effects and distortions caused by the electron-optical system of the microscope. Therefore the image interpretation is mostly based on results of computer simulation. If the initial structure motif is known (from X-ray analysis data, for example) or a structure is postulated, the matching procedure allows one to refine both the structural details and the experimental conditions under which the image has been obtained and to interpret the images of structure defects as well.

We should point out some disadvantages of this approach. Firstly, the trial-and-error nature of the simulation process leads to considerable expense of computer time and depends on the experience of the researcher. Secondly, it cannot be applied to the investigation of unknown structures.

The elaboration of direct structure-restoration methods seems to be attractive in this respect. The problem may be treated as consisting of two parts:

(*a*) correction for the transfer function of the microscope, *i.e.* restoration of the wave function at the exit plane of a crystal from the EM image(s);

(*b*) inversion of the dynamical diffraction, *i.e.* restoration of the lattice potential $V_e(r)$ from the exit plane wave function.

The dynamical scattering effects and the influence of the electron-optical system are therefore considered separately and this makes it possible to find independently the most efficient method for the solution of each problem.

Approaches aimed at restoration from the exit plane wave function include defocus series processing and transmission electron microscopy/scanning transmission electron microscopy (TEM/STEM) electron holography. Non-linear image processing methods have been suggested by Kirkland (1982,

* Now on leave: Department of Physics, Arizona State University, Tempe, AZ 85287-1504, USA.

0108-7673/91/060715-09$03.00

1984) for restoration from defocus series affected by noise. Their application to a Cu phthalocyanine structure has led to a good correlation with image simulation results and to improvement of interpretable resolution in the restored wave function. In the linear imaging approximation the exit plane wave function may be restored by the 'focus variation' method from the 3D Fourier analysis of defocus series. These include x, y coordinates in the image projection plane and defocus as a third coordinate (Van Dyck, 1990). The validity domain of this approach, however, still needs to be determined.

Electron off-axis holography (Lichte, 1988; Leuchtner, Lichte & Herrmann, 1989; Cowley, 1990) takes advantage of the interference between the two coherent beams, one of which is scattered by the object whereas the second one is passed through the vacuum. These beams are created by the Mollenstedt biprism inserted in the field-emission gun equipped electron microscope. Both the amplitude and the phase of the exit plane wave function may be restored from the Fourier analysis of the sidebands of a hologram. Nearly parallel illumination is used in TEM, whereas the two beams are focused in the object plane in the STEM case.

Electron crystallography methods aim at potential retrieval directly from a single EM image in a weak-phase-object approximation. This approximation, however, does not hold in most cases used in HREM. Therefore, only the qualitative information (location of projected potential peaks but not associated atom types) can be retrieved under certain conditions in this way (Goodman, Rae & Tulloch, 1988).

Less attention has been paid to the inversion of the dynamical electron diffraction. Two approaches based on the sequential approximation method and on the single Bloch-wave approximation have been proposed by Van Dyck (1985, 1990). The present paper follows the idea of an iterative solution to this problem and offers an alternative scheme for projected potential retrieval. Preliminary results suggested that a scheme was promising (Gribelyuk, 1989).

2. Method

The aim of the iteration procedure is to restore the lattice potential projection within the unit cell from the knowledge of the exit plane wave function. It is supposed that lattice parameters, orientation and crystal thickness are already determined.

2.1. *Algorithm*

I. The first estimation $V_1(\mathbf{r})$ of the potential is determined from the following expression:

$$\exp[-i\sigma V_1(\mathbf{r})t] * P_{t/2}(\mathbf{r}) = \Psi_e(\mathbf{r}). \quad (1)$$

Here $\mathbf{r} = (x, y)$ is a 2D vector in the image plane, σ is the interaction constant, t is the crystal thickness. $*$ denotes a convolution operation. The Fresnel propagation function (Cowley, 1975) is

$$P_t(\mathbf{r}) = (i/\lambda t) \exp(-i\pi r^2/\lambda t). \quad (2)$$

It should be noted that the lattice potential is considered here as a complex function. Within the multislice approach (1) implies that the whole crystal is treated as one slice and its potential is projected onto the middle plane of the crystal (Van Dyck, 1985). The numerical solution of (1) is most easily performed in reciprocal space using a convolution theorem. Instead of (1), one can use the phase object approximation (POA) or

$$\exp[-i\sigma V_1(\mathbf{r})t] * P_t(\mathbf{r}) = \Psi_e(\mathbf{r}) \quad (3)$$

can be used. The approximation (3) supposes that the potential is projected onto the entrance plane of the crystal. The choice of the starting approximation will be considered in detail in § 4.

II. At this step an estimation of the exit plane wave function $\Psi_n(\mathbf{r})$ is calculated from the current estimation of the projected potential $V_n(\mathbf{r})$.

Both Bloch-wave (BW) and multislice (MS) methods may be used for this purpose. From a computational point of view the desired operating memory is approximately proportional to $N \times N$ for BW and to N for MS with N being the number of reflections taken into account. Therefore, the application of the BW method is limited to structures with small lattice parameters. We aim at elaboration of a restoration scheme which may be applicable to any structure, including those containing defects. In this respect, the fast Fourier transform (FFT) multislice method (Ishizuka & Ueda, 1977) is preferable and therefore was used here.

In our multislice calculation the crystal is divided into k slices $\Delta z = t/k$ thick. Since only the projected potential in the crystal is known all the slices are considered as identical. The slice transmission function $q_n(\mathbf{r})$ is as follows:

$$q_n(\mathbf{r}) = \exp[-i\sigma V_n(\mathbf{r})\Delta z]. \quad (4)$$

Applying the basic multislice formula k times

$$\Psi_n^{(l+1)}(\mathbf{r}) = \Psi_n^{(l)}(\mathbf{r}) * P_{\Delta z}(\mathbf{r}), \quad (5)$$

one derives the estimation $\Psi_n(\mathbf{r})$ at the exit plane. Here $l = 0, 1, 2, \ldots, k-1$, the number of slices passed by the wave.

III. At this step a new estimation of the projected potential $V_{n+1}(\mathbf{r})$ is determined from the current estimations of the exit plane wave function $\Psi_n(\mathbf{r})$ and projected potential $V_n(\mathbf{r})$. The following expression is proposed:

$$\Psi_n(\mathbf{r}) \exp\{-i\sigma[V_{n+1}(\mathbf{r}) - V_n(\mathbf{r})]t\} = \Psi_e(\mathbf{r}). \quad (6)$$

This is illustrated in Fig. 1. The crystal with the model potential $V_e(\mathbf{r})$ is shown on the left and that with

estimated $V_n(\mathbf{r})$ potential on the right. The model wave function at the distance $r = t$ from the exit plane B may be written in the small-angle approximation:

$$^{l}\Psi(\mathbf{r}) = \Psi_e(\mathbf{r}) * P_t(\mathbf{r}). \tag{7}$$

If one requires the identity of wave functions in the A plane in both cases one should suppose that the electrons in Fig. 1(b) are travelling from plane B to plane A through a region with potential $\Delta V_n(\mathbf{r}) = V_{n+1}(\mathbf{r}) - V_n(\mathbf{r})$. Considering this region as one slice and projecting the $\Delta V_n(\mathbf{r})$ potential onto the B plane one obtains

$$\begin{aligned} ^{r}\Psi(\mathbf{r}) &= \Psi_n(\mathbf{r}) \exp[-i\sigma\Delta V_n(\mathbf{r})t] * P_t(\mathbf{r}) \\ &= {}^{l}\Psi(\mathbf{r}). \end{aligned} \tag{8}$$

This expression is equivalent to (6).

Once the new estimate for the potential is obtained step II is repeated and so on.

The iterations are stopped when the difference between successive values of the potential is smaller than a definite threshold. In order to estimate the result in a qualitative way one needs the half-tone representation of the potential. As a quantitative criterion the following expression may be used:

$$R = \max[|\Psi_e(\mathbf{r})/\Psi_n(\mathbf{r}) - 1|]. \tag{9}$$

It follows from (6) that R is proportional to $\max[\Delta V_n(\mathbf{r})]$ when the latter becomes small.

2.2. *Limitations*

The following problems will be treated below for determination of the validity domain of this method.

An experimental exit plane wave function $\Psi_e(\mathbf{r})$ is always known to a certain resolution $d = 1/u_0$ which is determined by instabilities and aberrations of the microscope. If the 'ideal' wave function $\tilde{\Psi}_e(\mathbf{u})$ has non-zero Fourier coefficients outside the circle $u = u_0$, in reciprocal space the iteration procedure based on the matching of wave functions $\Psi_n(\mathbf{r})$ and $\Psi_e(\mathbf{r})$ will lead to a potential different from $V_e(\mathbf{r})$, the true potential. One should therefore determine the highest spatial resolution of the retrieved potential where the restoration error does not exceed a certain threshold. Numerical estimations of this resolution are presented in § 4.

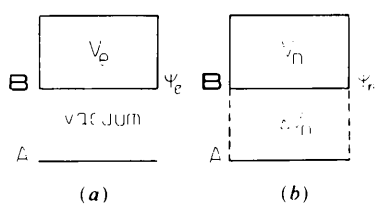

Fig. 1. Schematic representation of the iteration formula (6). Crystals with model $V_e(\mathbf{r})$ and estimated $V_n(\mathbf{r})$ potentials are shown in (a) and (b), respectively.

In any iteration method the main problems concern convergence rate and uniqueness of a solution. It is clear from the multislice expression (5) that inversion of dynamical diffraction is in general not unique: many different $V(\mathbf{r})$ functions are solutions of (5). The first approximation of the potential $V_1(\mathbf{r})$ is of critical importance in this respect; the procedure will converge to a solution which is the nearest to $V_1(\mathbf{r})$. The best available approximation (1), however, is rather limited relating to near phase objects. Our goal therefore is to specify the maximum object thickness up to which the proposed procedure still converges to a true solution. Uniqueness conditions are discussed in § 2.2.2 and a structure-independent criterion for estimation of the validity domain is proposed. These limits will be determined in § 4 on the basis of model calculations if (1) is used for the first approximation of potential $V_1(\mathbf{r})$. In addition, alternative expressions for $V_1(\mathbf{r})$ are tested in § 4 against convergence rate.

As can be seen from (1) and (6), both $V_1(\mathbf{r})$ and $\Delta V_n(\mathbf{r})$ can be derived only in the projection approximation. The exit plane wave function $\Psi_e(\mathbf{r})$ depends, however, on the full 3D potential $V_e(r, z)$. Therefore the restored potential $V(\mathbf{r})$ will differ from the projected true potential $V_e(\mathbf{r})$:

$$V_e(\mathbf{r}) = c^{-1} \int V_e(r, z)\, dz. \tag{10}$$

Here c is a lattice constant in the incident-beam direction. A full-scale estimation of HOLZ effects would require a multislice calculation of $\Psi_e(\mathbf{r})$ where slice projected potentials are derived from the full 3D potential $V_e(r, z)$ in the unit cell. The potential $V(\mathbf{r})$ should be restored from such a $\Psi_e(\mathbf{r})$ and compared with a true projected potential $V_e(\mathbf{r})$. Instead only the upper limit of the associated restoration error is estimated in § 4.

2.2.1. *Spatial resolution.* Let $\Psi_e(\mathbf{r})$ be known to $d = 1/u_0$ spatial resolution, *i.e.* in reciprocal space

$$\Psi_e(\mathbf{u}) = \tilde{\Psi}_e(\mathbf{u})A(\mathbf{u})$$

$$A(\mathbf{u}) = \begin{cases} 1 & |\mathbf{u}| \le u_0 \\ 0 & |\mathbf{u}| > u_0. \end{cases}$$

Here $\tilde{\Psi}_e(\mathbf{u})$ is the 'ideal' exit plane wave function, $A(\mathbf{u})$ is the effective aperture function, $d = 1/u_0$ is the spatial resolution. Since it is impossible to estimate the influence of this 'truncation' effect on the potential in a general way, let us consider this problem in the phase-object approximation. If one expands

$$\begin{aligned} \tilde{\Psi}_e(\mathbf{u}) &= F\{\exp[i\sigma V_e(r)t]\} \\ &= \delta(\mathbf{u}) - i\sigma V_e(\mathbf{u})t + (\sigma t)^2/2[V_e(\mathbf{u}) * V_e(\mathbf{u})] \\ &\quad - (\sigma t)^3/6[V_e(\mathbf{u}) * V_e(\mathbf{u}) * V_e(\mathbf{u})] + \ldots \end{aligned} \tag{11}$$

and leaves only the first two terms in the case $\varphi(\mathbf{u}) = |\sigma V_e(\mathbf{u})t| \ll 1$ it becomes clear that the potential will

change in the same way as the wave function:

$$V(\mathbf{u}) = \begin{cases} V_e(\mathbf{u}) & |\mathbf{u}| \le u_0 \\ 0 & |\mathbf{u}| > u_0. \end{cases} \quad (12)$$

If three terms are left in (11) the 'truncation' would require

$$-i\sigma V(\mathbf{u})t + (\sigma t)^2/2[V(\mathbf{u}) * V(\mathbf{u})] = 0 \quad \forall u: |\mathbf{u}| > u_0. \quad (13)$$

This results in the distortion of the whole $V_e(\mathbf{u})$ Fourier spectrum. The more terms that are essential in (11), the greater is the influence of the 'truncation' effect on the potential. The mixed terms of the $g(\mathbf{u}') = V(\mathbf{u}')V(\mathbf{u}-\mathbf{u}')$ type become large for $|\mathbf{u}| > u_0$ under either $\mathbf{u}' \to 0$ or $|\mathbf{u}-\mathbf{u}'| \to 0$ that results in a minimum in the intermediate region.

It follows from (4) and (6) that the Fourier spectrum of $\exp[i\sigma V_l(\mathbf{r})t]$ and of $\exp[-i\sigma\Delta V_n(\mathbf{r})t]$ are limited by $|\mathbf{u}| < u_0$ and $|\mathbf{u}| < 2u_0$, respectively. Thus, the best achievable spatial resolution of the restored potential is $d = 1/u_0$ and corresponds to $\varphi(\mathbf{u}) \ll 1$. However, $\varphi(\mathbf{u}) > 1$ in most practical cases, so in calculations (§ 4) the restored potential has been calculated with a number of different spatial resolution values and compared with the $V_e(\mathbf{r})$ model potential which was restricted to the same resolution. In this way the highest spatial resolution was found for which the given accuracy of restoration is guaranteed.

2.2.2. *Uniqueness of inversion.* The condition is given below under which (6) adequately describes the scattering process. Expression (6) may be obtained from the exact equation

$$\{q_n(\mathbf{r}) \exp[-i\sigma\Delta V_n(\mathbf{r})\Delta z] * P_{\Delta z}(\mathbf{r})\} q_n(\mathbf{r}) \times \exp[-i\sigma\Delta V_n(\mathbf{r})\Delta z] * \ldots = \Psi_e(\mathbf{r}). \quad (14)$$

If the correction term $\Delta V_n(\mathbf{r})$ is small enough that propagation effects are not essential:

$$\Psi_n^l(\mathbf{r}) \exp[-i\sigma\Delta V_n(\mathbf{r})t] q_n(\mathbf{r}) * P_{\Delta z}(\mathbf{r}) \simeq [\Psi_n^l(\mathbf{r}) q_n(\mathbf{r}) * P_{\Delta z}(\mathbf{r})] \exp[-i\sigma\Delta V_n(\mathbf{r})t] \quad (15)$$

for all l values. Here $\Psi_n^l(\mathbf{r})$ denotes the electron wave function corresponding to potential $V_n(\mathbf{r})$ after passing l slices. The better the first approximation $V_1(\mathbf{r})$ the smaller the correction term $\Delta V_n(\mathbf{r})$. As is known,

$$\alpha = \max[\varphi(\mathbf{r})] \quad (16)$$

may be considered as a figure of merit of the deviation of an exit plane wave function from the POA. This value will indicate the quality of the first approximation. Meanwhile, α is universal in the sense that potential, crystal thickness and the wavelength are combined. Therefore, determination of the validity domain of the method is performed in § 4 as a function of α. We expect that the results of this analysis will not be unduly dependent on the choice of model. In the evaluation of α we consider the projected potential $V_e(\mathbf{r})$ to be known to $d = 0{\cdot}1$ nm resolution. It will be shown that if the condition (15) fails the procedure may keep converging but the result does not necessarily correspond to the true potential (§ 4). This feature reveals that the solution of the direct problem is not unique with this method.

3. Program and structure model

The convergency check has been carried out on the hypothetical model of the UMo_5O_{16} oxide shown in Fig. 2. The structure is comprised of MoO_6 octahedra, elongated along the a and c axes. Octahedra are linked by corners within blocks, forming an ReO_3-like structure. Each block is $p = 2$ octahedra thick in the b-axis direction. The neighbouring blocks are linked by alternating U-O and Mo-O rows, elongated in the c-axis direction. The structure is orthorhombic with lattice constants $a = 0{\cdot}74$, $b = 1{\cdot}004$, $c = 0{\cdot}4115$ nm. The model exit plane wave function $\Psi_e(\mathbf{r})$ has been calculated in the (001) structure projection by the multislice method. The model potential $V_e(\mathbf{r})$ has been previously averaged over the c distance so that the occupancy factor for each cation within two slices of $\Delta z = 0{\cdot}2057$ nm thick has been set to 0·5. O atoms have not been taken into account. The elastic absorption has been introduced in the following way: $\mathrm{Im}[f_{Mo}(\mathbf{h})] = 0{\cdot}1 f_{Mo}(\mathbf{h})$, $\mathrm{Im}[f_U(\mathbf{h})] = 0{\cdot}19 f_U(\mathbf{h})$ for all the $\mathbf{h}$ reciprocal-lattice vectors. Here $f_U(\mathbf{h})$ and $f_{Mo}(\mathbf{h})$ denote the electron atomic scattering amplitudes for U and Mo cations, respectively. The Fourier coefficients $V_e(\mathbf{h})$ have been calculated for all $|\mathbf{h}| < 40\ \mathrm{nm}^{-1}$. Two 100 kV model wave functions $\Psi_e(\mathbf{r})$ have been calculated, *i.e.* for crystal thicknesses $t_1 = 1{\cdot}2345$ and $t_2 = 2{\cdot}0575$ nm. All the beams within the $|\mathbf{h}| < 20\ \mathrm{nm}^{-1}$ circle have been included but after multislicing the Fourier spectrum of $\Psi_e(\mathbf{r})$ has been cut to $|\mathbf{h}| < 10\ \mathrm{nm}^{-1}$ simulating the restricted resolution of the experimental wave function.

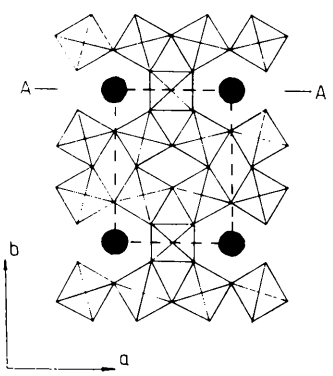

Fig. 2. Structure model of UMo_5O_{16} viewed along [001]. ● U; ⊕ MoO_6 octahedron. The unit cell is shown.

The computer program for structure retrieval has been written in FortranIV and installed on the IBM/370 operated under MVS. Expressions (1) and (6) have been used for calculation of successive potential estimations. Each iteration took 3 min CPU time for the complex FFT array size of 128×128 pixels and the six slices thick crystal, *i.e.* 20 s per slice in the multislice calculations.

4. Results

As was pointed out, the cutting of the exit plane wave-function Fourier spectrum $\Psi_e(\mathbf{r})$ leads to distortion of the corresponding potential $V_e(\mathbf{r})$. This effect is illustrated below for the UMo_5O_{16} structure. Firstly the 100 kV transmission function $\tilde{q}(\mathbf{r})$,

$$\tilde{q}(\mathbf{r}) = \exp[-i\sigma V_e(\mathbf{r})t],$$

was calculated for crystal thickness $t = 2{\cdot}0575$ nm, after which its Fourier spectrum was cut as follows:

$$Q(\mathbf{u}) = \begin{cases} \tilde{Q}(\mathbf{u}) & |\mathbf{u}| \le 10 \text{ nm}^{-1} \\ 0 & |\mathbf{u}| > 10 \text{ nm}^{-1}. \end{cases}$$

The potential $V(\mathbf{r})$ was calculated from the $Q(\mathbf{u})$ transmission function with spatial resolution $d = 0{\cdot}1$, $0{\cdot}2$, $0{\cdot}3$ nm, respectively, and compared with $V_e(\mathbf{r})$. In Fig. 3 the relative error between $V(\mathbf{r})$ and the corresponding $V_e(\mathbf{r})$ function near the cation sites along A-A (Fig. 2) is shown. Hereafter the origin was placed at the cation site. The A_r and A_{im} values are as follows:

$$A_r = |\text{Re}[V(\mathbf{r})]/\text{Re}[V_e(\mathbf{r})] - 1| \times 100\%$$

$$A_{\text{im}} = |\text{Im}[V(\mathbf{r})]/\text{Im}[V_e(\mathbf{r})] - 1| \times 100\%.$$

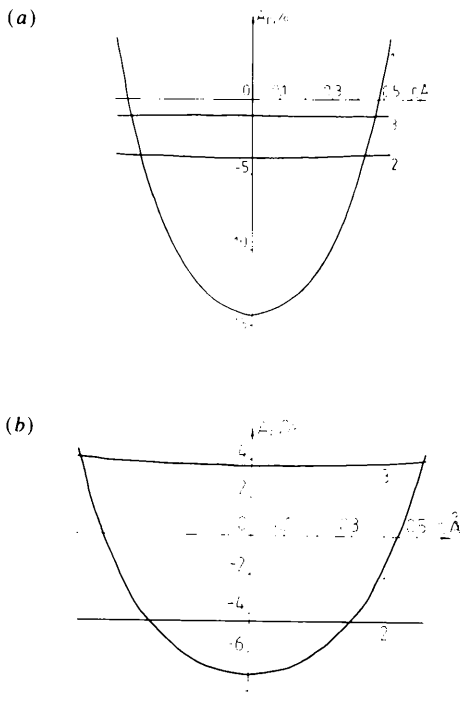

Fig. 3. Influence of the 'truncation' effect on the retrieved potential. The relative error A_r near (*a*) U and (*b*) Mo is shown as a function of resolution of the potential d: $d = 0{\cdot}1$ (curve 1), $0{\cdot}2$ (curve 2), $0{\cdot}3$ (curve 3) nm.

It can be seen that there is no strong correlation between A_r and the atomic scattering amplitude values. Actually, the A_r value for U cations may be both higher (curve 1) and lower (curves 2, 3) than that of Mo. The relative error A_r becomes smaller for lower resolution, although not linearly. The cutoff procedure is equivalent to an effective absorption. The imaginary part of the potential is responsible for this effect and increases two-three times near the atomic sites.

The restored potential for the $t = 1{\cdot}2345$ nm thick crystal is presented in Fig. 4 as a function of spatial resolution after ten iterations. This thickness corresponds to three unit cells and to $\alpha = 2{\cdot}4$. Expression (1) has been used for the first estimation; in iterations the crystal has been divided into six slices each $\Delta z = 0{\cdot}2057$ nm thick for calculation of $\Psi_n(\mathbf{r})$. The real part of the retrieved potential deviates from the true values of the model potential by not more than 5% near the atomic sites, with the spatial resolution of the potential $d > 0{\cdot}2$ nm. The iteration process converges rather fast: after only four iterations the A_r values varied within $0{\cdot}1\%$ (Fig. 4*d*). As can be seen from Fig. 4(*e*), the imaginary part cannot be restored due to the restricted resolution of the $\Psi_e(\mathbf{r})$ wave function. The real and imaginary parts of the potential are coupled in this method, therefore the accuracy of the $\text{Re}[V_e(\mathbf{r})]$ restoration cannot be made infinitely high for lower resolution. It should be mentioned that this result may be improved if the first estimation $\text{Im}[V_1(\mathbf{r})]$ is found from

$$\text{Im}[V_1(\mathbf{r})] = \beta \text{ Re}[V_1(\mathbf{r})] \qquad (17)$$

with the β parameter set to $0{\cdot}15$.

Now let us consider how the retrieved potential will vary if the first estimations are found from (3) or from the POA.

All three approximations lead to almost the same result ($\Delta A_r = 0{\cdot}1\%$) near the Mo sites if the spatial resolution of the potential $d > 0{\cdot}2$ nm. As should have been expected, the difference is larger near U sites (Fig. 5*a*). Expression (1) provides the best estimation of the retrieved potential (real part, curve 3). The POA and (3) lead to almost the same result (curve 2) which differs from the best one by $\Delta A_r = 0{\cdot}3\%$. Fig. 5(*b*) shows that the convergence is rather close for all approximations. One needs only one-two less iterations with (1) to achieve the same result as with (3) or the POA. Figs. 5(*c*), (*d*) reveal that approximation (1) does not necessarily provide the best

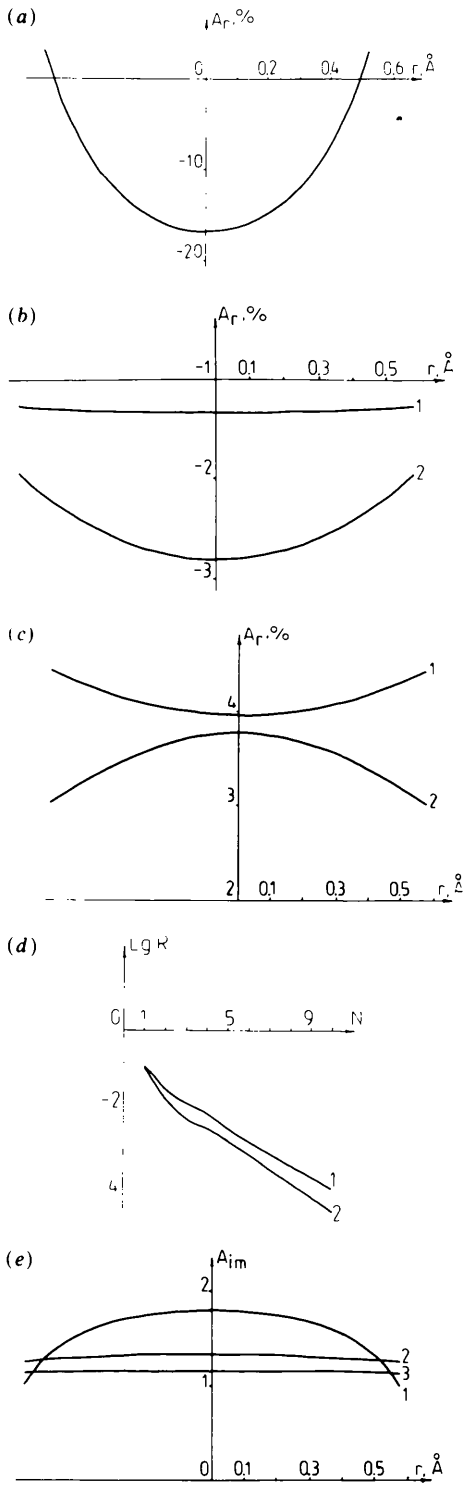

Fig. 4. Retrieved potential after ten iterations for $\alpha = 2{\cdot}4$ as a function of spatial resolution d. Relative error A_r at U site for (*a*) $d = 0{\cdot}1$ nm and (*b*) $d = 0{\cdot}2$ (curve 2), $0{\cdot}3$ (curve 1) nm. Relative error A_r at Mo for (*c*) $d = 0{\cdot}2$ (curve 2), $0{\cdot}3$ (curve 1) nm. (*d*) Convergence rate for iteration formulae (18) (curve 1) and (6) (curve 2). See expression (9) for definition of R_n. (*e*) Relative error A_{im} at U for $d = 0{\cdot}1$ (curve 1), $0{\cdot}2$ (curve 2), $0{\cdot}3$ (curve 3) nm.

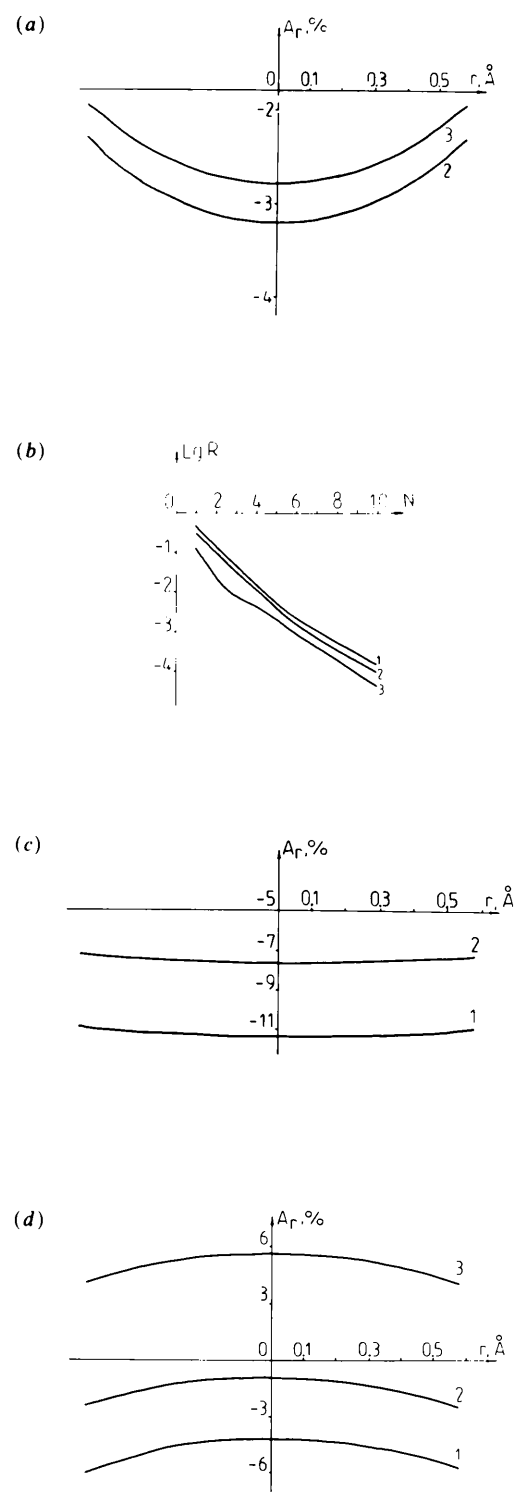

Fig. 5. Effect of the starting approximation on the retrieved potential ($\alpha = 2{\cdot}4$, spatial resolution $d = 0{\cdot}2$ nm). (*a*) Relative restoration error A_r at U after ten iterations. (*b*) Convergence rate. Relative error A_r at (*c*) U and (*d*) Mo after the first iteration. Curve 1, POA; curve 2, expression (3); curve 3, expression (1). Curves 1 and 2 nearly coincide in (*a*); $A_r < 0{\cdot}5\%$ for expression (1) in (*c*).

estimation of the real part Re $[V_1(\mathbf{r})]$ of the potential compared with those of (3) and POA. This is not inconsistent, however, because (1) gives the best estimation of the full potential, but not of each part separately.

Thus, one may apply any of the mentioned approximations for thin crystals or structures formed by light atoms ($\alpha < 2{\cdot}5$). In other cases approximation (1) is preferable.

Recently another iteration formula was proposed (Van Dyck, 1985):

$$\exp[-i\sigma V_{n+1}(\mathbf{r})t] - \exp[-i\sigma V_n(\mathbf{r})t] = \Psi_e(\mathbf{r}) - \Psi_n(\mathbf{r}). \quad (18)$$

This is similar to the sequential approximations method of searching for $f(x) = x$ equation roots if one sets

$$x_{n+1} = \exp[-i\sigma V_{n+1}(\mathbf{r})t]$$
$$f(x_n) = \Psi_e(\mathbf{r}) - \Psi_n(\mathbf{r}) + x_n. \quad (19)$$

The sign in the exponent has been changed to the opposite one in comparison with the original because here and in Van Dyck (1985) different expressions for the incident plane wave have been used [see sign conventions in Self, O'Keefe, Buseck & Spargo (1983)]. This procedure enables the retrieval of the structure potential of an SiF_4 crystal with $t < 1{\cdot}6$ nm ($\alpha < 1{\cdot}5$). Both the model wave function and its estimations have been calculated by the real-space method (Van Dyck, 1985). The sequential approximations method requires that initial estimation should be close enough to the true solution. Estimating the validity domain of (18) we applied it to a 1·2 nm thick crystal of UMo_5O_{16}, which corresponds to $\alpha = 2{\cdot}4$. Our calculations reveal that (18) still provides reliable restoration results. The restoration errors are almost on the same scale as (6), but the convergence rate of (18) is lower (Fig. 4*d*).

As has been mentioned, the assumption of equal slices in the multislice calculations of the wave function $\Psi_n(\mathbf{r})$ may cause a restoration error, *i.e.* the difference between restored potential $V(\mathbf{r})$ and the true projected potential $V_e(\mathbf{r})$. One needs a full $V_n(\mathbf{r}, \mathbf{z})$ potential, but not its projection $V_n(\mathbf{r})$ in a crystal for accurate analysis.

We aim at estimation of an upper limit of restoration errors which result from neglect of HOLZ effects. For this purpose we created an artificial non-uniform distribution of potential in a 1·2 nm thick UMo_5O_{16} crystal along **z**, the beam direction, in the following way. The unit cell of UMo_5O_{16} was divided into two slices in the (001) projection. The U and Mo atoms between octahedral blocks as well as half of the Mo atoms in blocks were set in the upper slice with the other Mo atoms in the bottom one. In evaluation of the slice projection potential only those atoms which were located in the slice were taken into account. Therefore, a step-like potential distribution along the z direction for each atom in the unit cell was assumed; it has non-zero values only in one of two slices within the unit cell. Apparently, the difference between projected potential distributions of two slices is larger here than in the original model (Fig. 2). The projected potential $V_e(\mathbf{r})$ within the unit cell remains, however, the same as before. The 100 kV model wave function was calculated for the crystal thickness $t = 1{\cdot}2345$ nm with the final spatial resolution $d = 0{\cdot}1$ nm. The restoration of potential from such a model led to an error as low as $\Delta A_r < 8{\cdot}5\%$ near atom sites (Fig. 6). This error is apparently larger than the actual error resulting from neglection of HOLZ effects and becomes less for structures formed by light atoms.

Thus, the method allows one to retrieve the real part of the potential with an error of less than 10% if $\alpha < 2{\cdot}5$.

Let us estimate the range of α values that guarantees convergence to the true result with this method. For this purpose, iterations have been performed with the model wave function calculated for the 2·0575 nm thick crystal ($\alpha = 4{\cdot}6$). The slice thickness $\Delta z = 0{\cdot}2057$ nm was used for both the model wave function $\Psi_e(\mathbf{r})$ and its estimations $\Psi_n(\mathbf{r})$.

The $V_1(\mathbf{r})$ potential estimation obtained from (1) does not correlate with the model potential (Fig. 7*a*): its real part has a minimum instead of a peak at U sites. Estimations $\Psi_n(\mathbf{r})$ converge rapidly to the model wave function $\Psi_e(\mathbf{r})$. Nevertheless, the restored potential $V(\mathbf{r})$ remains as far from the model $V_e(\mathbf{r})$ as the first approximation $V_1(\mathbf{r})$. This feature proves that the solution of the direct problem is not unique with this method. The condition (15) has not been satisfied in this case, so the $V_n(\mathbf{r})$ estimations converged to one of the 'false' solutions.

Thus, the requirement that the correction value has to be small imposes serious restrictions on the validity domain of the procedure.

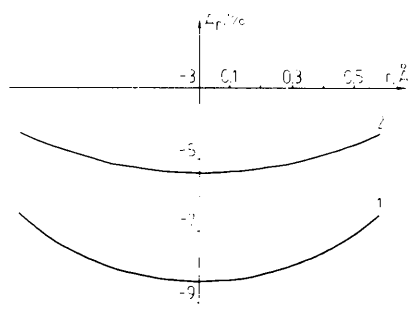

Fig. 6. Upper limit of the restoration error resulting from neglect of HOLZ effects. Relative error A_r at U as a function of spatial resolution of potential d is shown: $d = 0{\cdot}2$ (curve 1), 0·3 (curve 2) nm.

The following explanation may be proposed for the failure of (15). The difference between the estimation $V_1(\mathbf{r})$ and the model potential $V_e(\mathbf{r})$ is caused by incomplete treatment of dynamical scattering effects in (1). Within the multislice method this means that the first approximation treats the crystal as consisting of one slice; an exact solution corresponds to a fine slicing of a crystal. For multislice calculation of $\Psi_1(\mathbf{r})$ very thin slices ($\Delta z = 0{\cdot}2057$ nm) were used whereas the potential $V_1(\mathbf{r})$ was obtained from $\Psi_e(\mathbf{r})$ in a 'one-slice' approximation (1). Therefore, large differences can be expected between $\Psi_1(\mathbf{r})$ and $\Psi_e(\mathbf{r})$, *i.e.* the condition (14) must have already failed in the evaluation of $V_2(\mathbf{r})$.

To make this difference smaller we proceed in the following way. Once the first approximation $V_1(\mathbf{r})$ is found a crystal is divided into two slices and iterations are performed until convergence of $\Psi_n(\mathbf{r})$ and $\Psi_e(\mathbf{r})$ is achieved. At the next step a crystal is divided into three slices and iterations are repeated *etc.* Meanwhile, the difference $\Delta(\mathbf{r}) = \Psi_n(\mathbf{r}) - \Psi_e(\mathbf{r})$ is smaller at each step with respect to previous iterations so the condition (15) may be satisfied. We expect convergence of potential estimation $V_n(\mathbf{r})$ to a true solution $V_e(\mathbf{r})$ as a slice thickness Δz is decreased (or a number of slices is increased).

Results of the potential retrieval are shown in Figs. 7(*b*), (*c*). The crystal was subsequently subdivided into $n = 1, 2, 3, 4, 6, 10$ slices. At each stage iterations were performed until the desired $R < 0{\cdot}001$ accuracy was achieved between $\Psi_n(\mathbf{r})$ and $\Psi_e(\mathbf{r})$ [see (9)]. Note that $\Psi_n(\mathbf{r})$ denotes here the result of iterations if a crystal is divided into n slices for multislice calculation. The estimation of $\mathrm{Im}[V_1(\mathbf{r})]$ has been found from (17). An accuracy of the retrieved potential as high as $A_r < 10\%$ was achieved near atomic sites after 73 iterations if one considers a potential calculated with spatial resolution $d > 0{\cdot}2$ nm. The imaginary part of the potential cannot be retrieved. It should be noted that if the estimation of $\mathrm{Im}[V_1(\mathbf{r})]$ is found from (1) (both real and imaginary parts), the accuracy of the retrieval becomes lower: $A_r < 17\%$. The calculations reveal that such an accuracy is preserved until $\alpha < 5$. The restoration error grows quickly for $\alpha > 5$ with this method.

The next problem concerns the optimum spatial resolution to which the estimation $\Psi_n(\mathbf{r})$ should be calculated by the multislice method. The finite number of beams in the multislice calculation introduces wrap-around errors in the estimated wave function. Until now the resolution of $\Psi_n(\mathbf{r})$ has been restricted to $d = 0{\cdot}1$ nm, *i.e.* to the spatial resolution of the model wave function $\Psi_e(\mathbf{r})$. The reason for such a restriction was the distortion of slice transmission function $q(\mathbf{r})$ by the 'truncation' effect of $\Psi_e(\mathbf{r})$. It is important to estimate the relationship between these two effects and to check whether the multislicing with higher resolution and subsequent cutoff to $d = 0{\cdot}1$ nm could lead to a better result for the restoration procedure.

The multislice calculations of $\Psi_n(\mathbf{r})$ were initially performed with $u < 20\ \mathrm{nm}^{-1}$ and the estimated wave function was restricted after that to $u < 10\ \mathrm{nm}^{-1}$ before applying the iteration formula (6). The model wave function derived earlier for the 2·0575 nm thick crystal was used. The result of restoration was worse in this case than that presented in Fig. 7. This proves that the 'truncation' effect of $\Psi_e(\mathbf{r})$ affects the estimated wave function more than wrap-around errors do.

Thus, the calculation of $\Psi_n(\mathbf{r})$ should be performed with the same spatial resolution as the 'experimental' wave function is known.

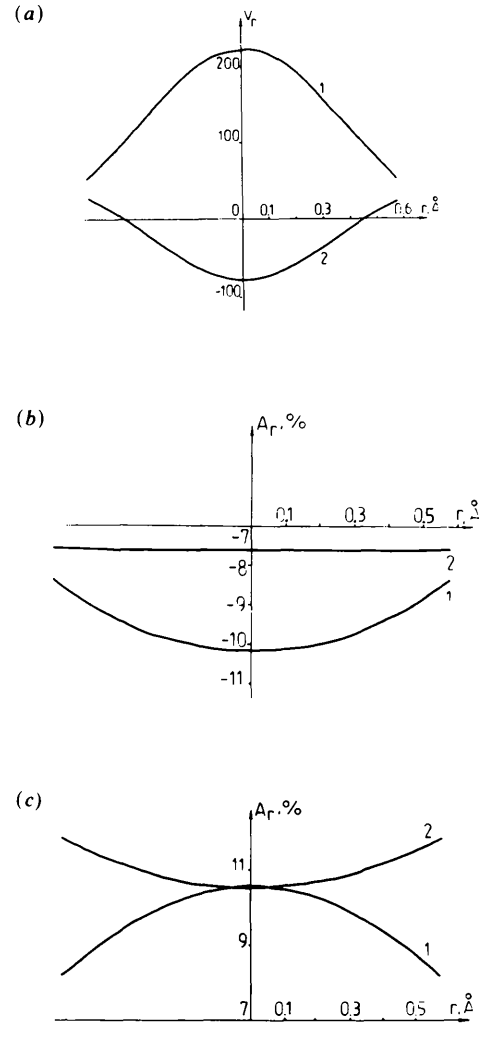

Fig. 7. Potential retrieval for $\alpha = 4{\cdot}6$. (*a*) True profile of $\mathrm{Re}[V_e(\mathbf{r})]$ (curve 1) and its first estimation (curve 2) at U. Relative error A_r at (*b*) U and (*c*) Mo after 73 iterations as a function of spatial resolution of the potential d: $d = 0{\cdot}2$ (curve 1); 0·3 (curve 2) nm.

The author is indebted to Dr N. D. Zakharov, Institute of Crystallography, Moscow, and Dr J. L. Hutchison, Department of Materials, University of Oxford, for valuable discussions and reading of the manuscript.

References

COWLEY, J. M. (1975). *Diffraction Physics.* Amsterdam: North Holland/American Elsevier.
COWLEY, J. M. (1990). *Ultramicroscopy*, **34**, 293-297.
GOODMAN, P., RAE, S. C. & TULLOCH, P. A. (1988). *Acta Cryst.* A**44**, 905-912.
GRIBELYUK, M. A. (1989). Proc. XII Eur. Crystallogr. Meet., Moscow, Vol. 1, p. 112.
ISHIZUKA, K. & UEDA, N. (1977). *Acta Cryst.* A**33**, 740-749.
KIRKLAND, E. J. (1982). *Ultramicroscopy*, **9**, 45-64.
KIRKLAND, E. J. (1984). *Ultramicroscopy*, **15**, 151-172.
LEUCHTNER, TH., LICHTE, H. & HERRMANN, K.-H. (1989). *Phys. Status Solidi A*, **116**, 113.
LICHTE, H. (1988). *Ultramicroscopy*, **20**, 293-304.
SELF, P. G., O'KEEFE, M. A., BUSECK, P. R. & SPARGO, A. E. C. (1983). *Ultramicroscopy*, **11**, 35-52.
VAN DYCK, D. (1985). In *Advances in Electronics and Electron Physics*, edited by P. W. HAWKES, pp. 295-355. New York: Academic Press.
VAN DYCK, D. (1990). *Proc. XII Int. Congr. for Electron Microscopy, Seattle*, Vol. 1, pp. 64-65. San Francisco Press.

Acta Cryst. (1991). A**47**, 723-727

How to Calculate Planarity Restraints

BY A. G. URZHUMTSEV

Research Computing Center, USSR Academy of Sciences, Pushchino, Moscow region, 142292 *USSR*

(*Received* 25 *December* 1990; *accepted* 29 *May* 1991)

Abstract

Planarity of some atomic groups is one of the important stereochemical features of a model under refinement. A planarity restraint is usually included in the functional to be minimized. A new method of *analytical* calculation of the exact gradient value is suggested for the standard function [Schomaker, Waser, Marsh & Bergman (1959). *Acta Cryst.* **12**, 600-604] which controls planarity in the most direct way. This approach makes it possible to refine the optimum plane orientation at the same time as atomic coordinates.

I. Introduction

The procedure for atomic model refinement in protein crystallography is (or may be reduced to) a minimization of some functional. This functional is usually a sum of simple criteria, each of which is responsible for a special type of restraint. One of the most important stereochemical restraints imposed on a number of atomic groups is a planarity restraint. It usually consists of items of the same type, each of which is a function of the coordinates of the atoms which should lie on the plane. The function value increases with planarity distortion.

Various approaches are known to define such a function. In one of them planarity is controlled by means of bond lengths, bond angles *etc.* (Waser, 1963; Levitt & Lifson, 1969; Hermans & McQueen, 1974; Ten Eyck, Weaver & Matthews, 1976; Chambers & Stroud, 1977). Another method is the introduction of one (Dodson, Isaacs & Rollett, 1976) or two (French, 1975; Tomlin, 1987) dummy atoms at a distance from the best plane through a group of atoms and changing the distances between atoms of the group and the dummy atoms. The third approach (used, for example, in a program by Hendrickson & Konnert, 1980) is based on the calculation of a root-mean-square deviation of atoms from the best plane (Schomaker *et al.*, 1959). This approach seems the most suitable of the three, since the two others define planarity requirements in a less direct way and are not always effective (the latter was demonstrated by Haneef, Moss, Stanford & Borkakoti, 1985). But one should keep in mind when dealing with the last method that it requires the calculation of the best plane parameters. Usually, they are determined with the iterative procedure of Frazer, Duncan & Collar (1938), and the best plane orientation is difficult to refine. To avoid the problem of the choice of the best plane, Haneef *et al.* (1985) suggested a new variant of this approach that does not need optimal plane parameters and makes use of a very simple criterion.

In spite of the evident advantages, the criterion of Haneef *et al.* (1985) has an important feature: it distorts the atomic group, forcing atoms to move towards the centre of the group. This effect is explained in the present work. Of course, other functionals, *e.g.* bond-length restraints, prevents the group from collapsing, but we could not then clearly recognize which functional is responsible for planarity only

0108-7673/91/060723-05$03.00